JOURNAL OF Applied Polymer SCIENCE

Optimization of Mechanical Performance of Compatibilized Polypropylene/Poly(ethylene terephthalate) Blends via Selective Dispersion of Halloysite Nanotubes in the Blend

Tengfei Lin,[1] Lixin Zhu,[1] Tao Chen,[1] Baochun Guo[1,2]

[1]Department of Polymer Materials and Engineering, South China University of Technology, Guangzhou 510640, People's Republic of China

[2]State Key Laboratory of Pulp and Paper Engineering, South China University of Technology, Guangzhou 510640, People's Republic of China

Correspondence to: B. Guo (Email: psbcguo@scut.edu.cn) or L. Zhu (pszlx@scut.edu.cn)

ABSTRACT: Many recycled plastics are the polypropylene (PP)/poly(ethylene terephthalate) (PET) blends with PET as the minor component. The modification of such kinds of PP/PET blends for higher performance is essential as PP and PET are not thermodynamically compatible. In this study, the elastomer, SEBS-*g*-MAH, and the inorganics, halloysite nanotubes (HNTs) are chosen as the modifiers for the modification of a model PP/PET blend (90/10). The mechanical performance of such blend is optimized by the selective dispersion of the nanotubular HNTs into the interfacial region of the blends via a two-step process. Compared with the control one, the overall mechanical properties of the blend are substantially improved. The crystallization of PP in the blend is also facilitated by the selective dispersion of HNTs and the folding surface free energy is substantially increased. The substantially improved mechanical performance is interpreted according to the formation of the unique morphology. This study provides new insight in improving the performance of polymer blends via selectively dispersing the nanosized inorganics in the blend. © 2012 Wiley Periodicals, Inc. J. Appl. Polym. Sci. 129: 47–56, 2013

KEYWORDS: polyesters; polyolefins; morphology; elastomers; inorganic polymers

Received 1 July 2012; accepted 1 October 2012; published online 3 November 2012
DOI: 10.1002/app.38700

INTRODUCTION

Polypropylene (PP)/poly(ethylene terephthalate) (PET) blends with PP as the major phase are widely studied and used in many application areas, especially in packaging materials.[1–6] For example, flexible intermediate bulk containers (FIBCs), a typical PP/PET blend in which the PET content is about 10 wt %, are widely used in the industry for the transport and storage of powders, granules, or pellets.[7–9] Owing to large quantity of FIBC and the difficulties in removing the PET from FIBC, it is important to develop an effective method for the recycling of FIBC directly. It is well known that PP and PET are immiscible thermodynamically, and directly blending may lead to poor compatibility and low impact strength. Therefore, the compatibilization of recycled FIBC is essential.

The compatibilizations of PP/PET have been highlighted during the past two decades. Various compatibilizers, such as PP grafts,[10–15] polyethylene-octene elastomer (POE) grafts,[16] linear low-density poly(ethylene) grafts,[17] styrene-*b*-(ethylene-*co*-butylene) (SEBS) grafts,[17–19] and styrene-*b*-(ethylene-*co*-propylene) (SEP) grafts[19] have been attempted and some successes have been made. However, the enhancement of impact strength has been obtained with the sacrifice of the modulus owing to the inclusion of functionalized elastomers into PP/PET blends.[16] The increase in toughness without sacrificing the modulus is especially important in many applications. Therefore, further addition of nanosized inorganics into the compatibilized blends to balance toughness and modulus has been attempted as it has been noticed that inorganics can effectively increase the modulus of polymer.[20–22] Besides, the utilization of inorganics encapsulated with elastomer has been found to be effective to the simultaneous retention of modulus and toughness.[23–26]

In this study, a model blend for FIBC was prepared by blending PP and PET in a proportion of 90 and 10 wt %. SEBS-*g*-MAH, a maleic anhydride-grafted SEBS elastomer, was selected as the compatibilizer for the blend after cautiously comparing with ethylene–acrylic ester–maleic anhydride terpolymer. It has also been verified that SEBS-*g*-MAH was more effective in improving the toughness of the PP/PET blends for its chemical structure and the presence of PS blocks.[17] To further improve the overall performance, halloysite nanotubes (HNTs) were used to modify the compatibilized PP/

PET blend. HNTs, with the ideal chemical formula of $Al_2Si_2O_5(OH)_4 \cdot nH_2O$, are chemically similar to kaolinite.[27] Previously, HNTs have been demonstrated to be promising in the reinforcement of different polymers.[28–34] To optimize the mechanical performance, a two-step process was used to prepare the blend with the controlled dispersion of HNTs. The morphology, mechanical properties, and crystallization of the blends prepared by the two-step method and the regular single-step method have been studied and compared. The substantially improved mechanical properties in the blends prepared by the two-step method have been correlated to the unique selective dispersion of HNTs in the interfacial region and the changed crystallization behavior.

EXPERIMENTAL

Materials

PP, with trademark 11040-31, was made in Saudi Arabia. PET, intrinsic viscosity: 0.9 dL/g. SEBS-*g*-MAH, with trademark M1913, was manufactured by Asahi Kasei, Japan. HNTs were mined from Hubei Province, China and purified according to the established method.[35]

Preparation of the PP/PET Blends

PP, SEBS-*g*-MAH, and HNTs were dried at 80°C for 12 h in oven. PET was dried in a vacuum drum drying oven (2 h at 90°C and then dried at 120°C for 24 h).

In the single-step process, both SBES-*g*-MAH and HNTs were directly compounded with PP/PET, whereas in the two-step process, SEBS-*g*-MAH and HNTs were first mixed at 120°C for 10 min in a two-roll mixer and then blended with PP/PET following the same procedure as the single-step process. The sample codes of *Sx* and *Tx* mean the compatibilized PP/PET blend prepared by single-step process and two-step process, respectively. The HNTs content in these blends is *x* wt % relative to the amount of PP and PET. We have carefully studied the compatibilizing effect of SEBS-*g*-MAH in different contents preliminarily. The content of SEBS-*g*-MAH is therefore chosen as 5 wt % relative to the amount of PP and PET in this study for the consideration of balanced toughness and modulus.

Both the melt blending of single-step process and two-step process compounds were done with a twin-screw extruder. The temperature profile from the barrel to die was 180/260/265/265/265/265/265/265265/260°C. The screw speed was 100 rpm.

The pelletized extrudates were dried in a vacuum oven and then injection molded for the mechanical testing. The temperature profile from the barrel to die was 180/265/265/270°C.

Characterization of Mechanical Properties

The specimens for the mechanical testing were conditioned for 24 h at room temperature. The tensile strengths, flexural strengths, and flexural modulus of the composites were measured using U-CAN UT-2060 (Taiwan) instrument according to ISO 527: 1993 and ISO 178: 1993, respectively. The Izod impact strengths were measured on an XJ-40A impact tester according to ISO 180: 1993.

Morphology

The impact-fractured surfaces of the composites were characterized with an EVO 18 (Carl Zeiss, Germany) scanning electron microscopy (SEM). TEM observations for the ultramicrotommed samples (Leica EM UC6; Leica, Wetzlar, Germany) were carried out by JEM-100CX II microscope at an accelerating voltage of 30 kV. The ultramicrotommed samples were stained by using ruthenium tetroxide (RuO_4) before TEM observations. Elemental analyses of the interfacial region component of the samples were characterized by TEM-associated energy-dispersive spectrometer (EDS) analysis (JEM-2100F). Morphologies of the crystallites of the samples were observed with an Olympus BX51 polarized light microscopy (PLM). The samples were heated to 260°C and kept for 5 min to eliminate the thermal history, and then cooled to 120°C at a rate of 5°C/min for the PLM observation.

Differential Scanning Calorimetry

Differential scanning calorimetry (DSC) data were measured by TA Q20 using nitrogen as purging gas. The samples were heated to 290°C at ramping rate of 20°C/min and kept at 290°C for 3 min to eliminate the thermal history before it is cooled down to 50°C at a rate of 10°C/min. Then, the samples were reheated to 290°C at a ramping rate of 10°C/min. The endothermic and exothermic flows were recorded as a function of time.

To determine the nonisothermal crystallization behavior of PP and PP/PET blends, the samples were heated to 200°C at a ramping rate of 20°C/min, and then the samples were kept at 200°C for 5 min to eliminate the thermal history before they were cooled down to 50°C at the rates of 5, 10, 15, and 20°C/min, respectively. The exothermic flows were recorded as a function of temperature.

To determine the equilibrium melting point of the samples, isothermal crystallization was also performed. The samples were heated to 200°C at a ramping rate of 20°C/min and kept at 200°C for 5 min to eliminate the thermal history. Then, the samples were quenched to the crystallization temperature (120, 122, 124, and 126°C) and kept for at least 30 min and then reheated to 200°C at a ramping rate of 20°C/min. The endothermic and exothermic flows were recorded as a function of time.

The crystallinity was calculated based on the endothermic enthalpy (ΔH_f) as follows.

$$Xt = \frac{\Delta H_f}{\Delta H_f^0 \times C} \quad (1)$$

where ΔH_f and ΔH_f^o are the endothermic enthalpies of the sample and the PP with crystallinity of 100%, respectively. C is the PP weight percentage in the composite. The value of ΔH_f^o is taken as 209 J/g.[36]

Calculation of Hoffman–Lauritzen Parameters by Nonlinear Isoconversional Method

As we know, Avrami equation can only evaluate the overall rate and activation energy of the nonisothermal crystallization. The single value of the activation energy could not adequately represent the crystallization process. Therefore, the isoconversional method has been developed to eliminate these problems and the physically meaningful parameters for the crystallization could be evaluated.

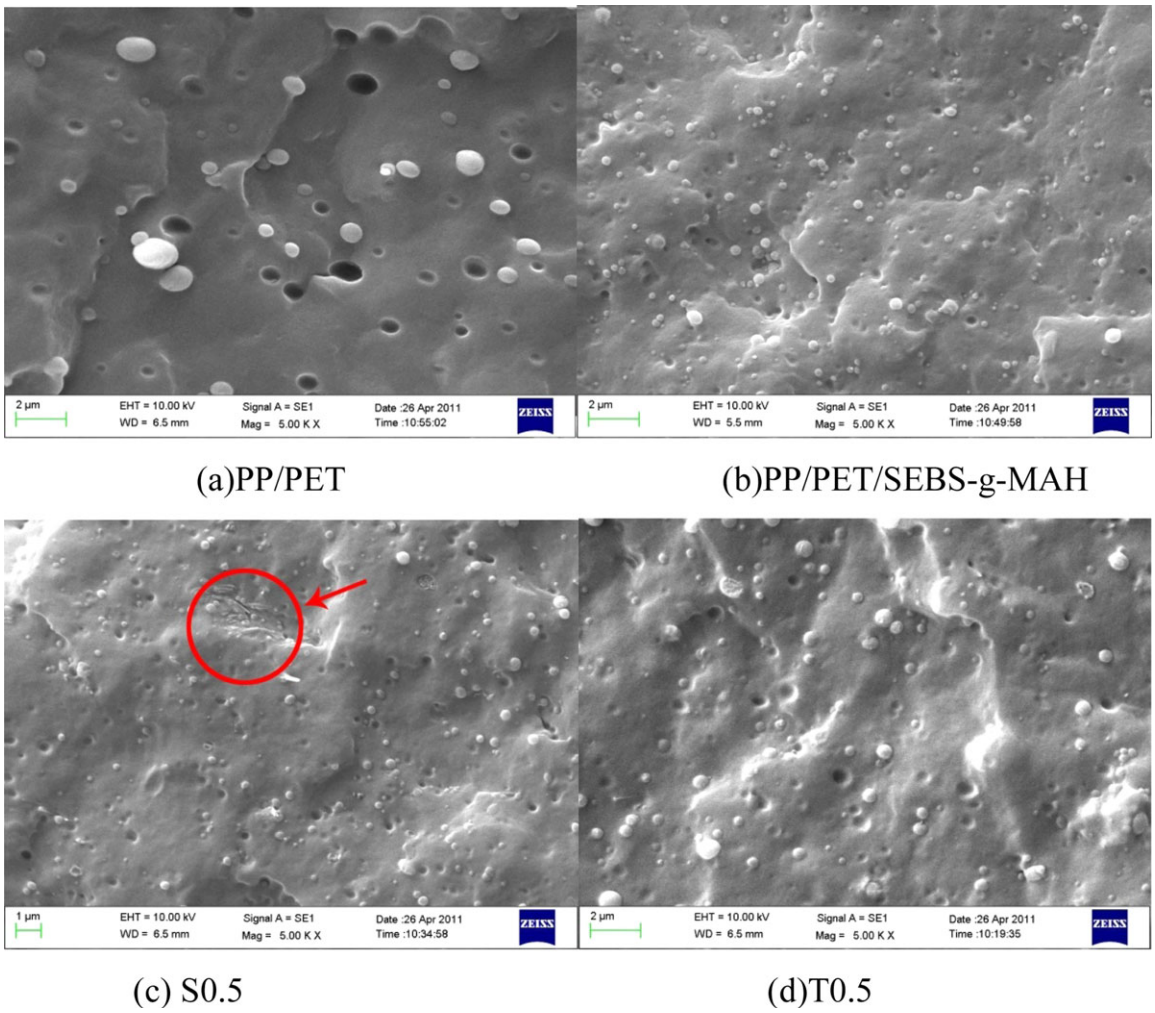

Figure 1. Comparison of different morphologies of the fractured surfaces. HNT aggregates are marked with the red cycle. [Color figure can be viewed in the online issue, which is available at wileyonlinelibrary.com.]

Based on the Hoffman–Lauritzen theory,[37] that the linear growth rate of a polymer crystal, G depends on temperature, T as follows.

$$G = G_0 \exp\left(\frac{-U*}{R(T - T_\infty)}\right) \exp\left(\frac{-K_g}{T\Delta T_f}\right) \quad (2)$$

where G_0 is the pre-exponential factor, U^* is the activation energy of the segmental jump, $\Delta T = T_m^0 - T$ is the undercooling, $f = 2T/(T_m^0 - T)$ is the correction factor, T_∞ is a hypothetical temperature at which viscous flow ceases and is usually taken 30 K below the glass transition temperature (T_g, in this study T_∞ takes 253.15 K for neat PP and their composites).[37] The kinetic parameter K_g has the following form.

$$K_g = \frac{nb\sigma\sigma_e T_m^0}{\Delta h_f^0 k_B} \quad (3)$$

where n takes the value of 4 in this study; b is the distance between two adjacent fold planes (for PP $b = 6.56 \times 10^{-10}$ m); σ and σ_e are the lateral and folding surface-free energy ($\sigma = 8.79 \times 10^{-3}$ J/m^2), T_m^0 is the equilibrium melting temperature, Δh_f^0 is the heat of fusion per unit volume of crystal (1.34×10^8 J/m^3), k_B is the Boltzmann constant.[38] The parameters U^* and K_g are usually determined by measuring the growth rate microscopically in a series of nonisothermal runs and substituting the measured value in rearranged eq. (2).

$$\ln G + \frac{U*}{R(T - T\infty)} = \ln G_0 - \frac{K_g}{T\Delta T_f} \quad (4)$$

In narrow temperature region, an explicit dependence of effective activation energy (E) on T can be derived from eq. (4) as follows.[39]

$$E_\alpha(T) = -R\frac{d\ln G}{dT^{-1}} = U*\frac{T^2}{(T - T_\infty)^2} + K_g R\frac{(T_m^0)^2 - T^2 - T_m^0 T}{\Delta T^2 T} \quad (5)$$

where E_α represents the effective activation energy when the crystallinity degree is α. According to the theory of Hoffman–Weeks,[40] the equilibrium melting temperature (T_m^0) can be

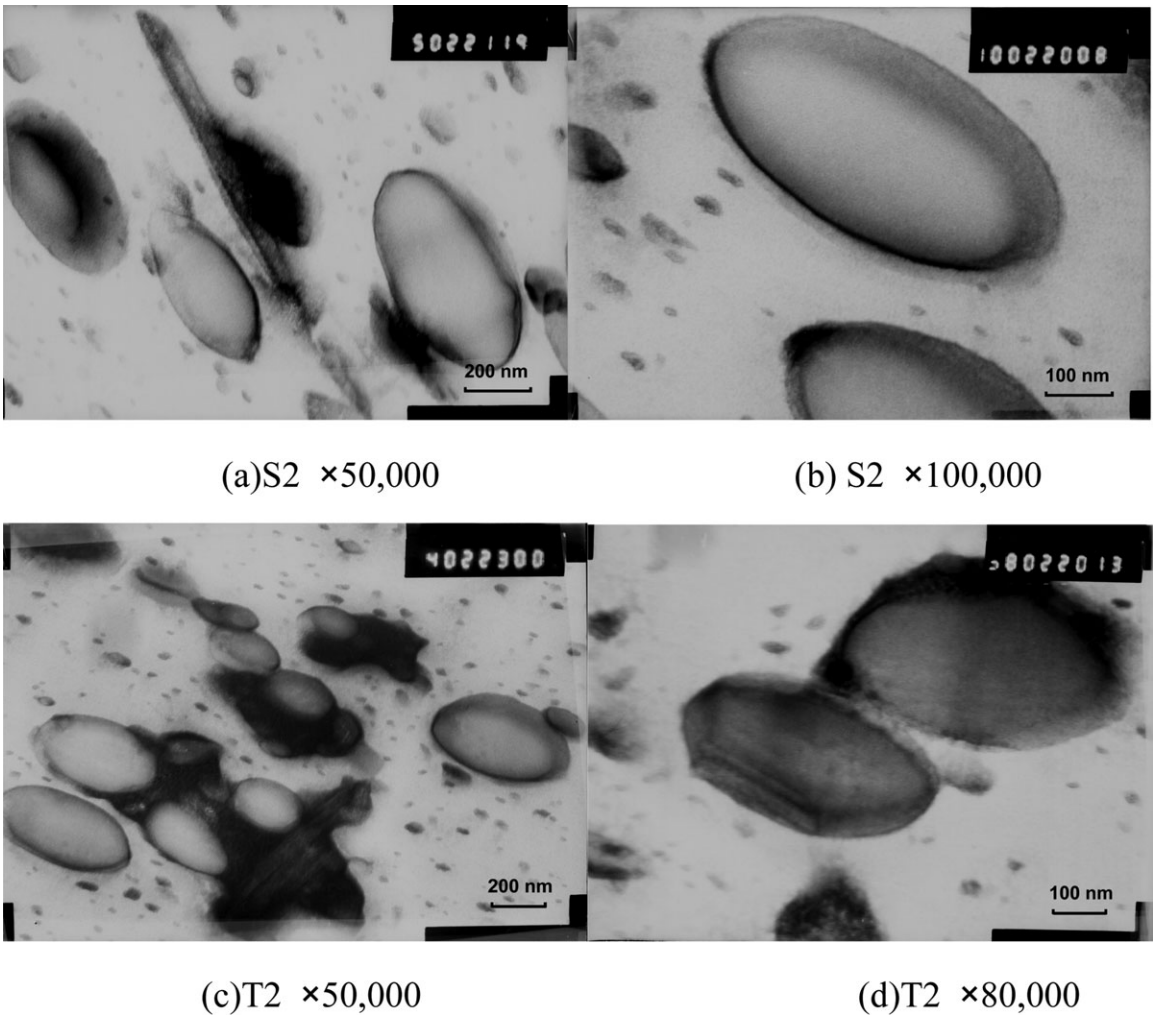

Figure 2. TEM micrographs of the ultramicrotommed samples.

obtained by linear extrapolation of T_m versus T_c data to intersect the line $T_m = T_c$ and the intersection point is the T_m^0.

Based on nonlinear isoconversional method,[41] the effective activation energy for the nonisothermal crystallization is calculated according to eq. (6) and the specific derivation process can be figured out by using as reference.[42,43]

$$\Omega(E_\alpha) = \min\left|\sum_{i=1}^{n}\sum_{j\neq i}^{n}\frac{\varphi_j \bullet I(E_\alpha, T_{\alpha,i})}{\varphi_i \bullet I(E_\alpha, T_{\alpha,j})} - n(n-1)\right| \quad (6)$$

Here:

$$I(E_\alpha, T_\alpha) = \int_{T_0}^{T_\alpha} \exp\left(\frac{-E_\alpha}{RT_\alpha}\right) dT \quad (7)$$

This integral is determined with the help of a Doyle's approximation.[44]

$$I(E_\alpha, T_\alpha) \cong \frac{E_\alpha}{R}\exp\left(-5.331 - 1.052\frac{E_\alpha}{RT_\alpha}\right) \quad (8)$$

where ϕ stands for the cooling rate; n represents the number of cooling rates and in this study it is 4. By substituting a series of different ϕ_i, $T_{\alpha,i}$ ($i = 1, 2, \ldots n$) estimated at the same α on the DSC curves into eq. (6), we can obtain the minimum value of E_α.

RESULTS AND DISCUSSION

Morphological Observations

The SEM images of the fractured surfaces of impact specimens are shown in Figure 1. It can be clearly seen that without the compatibilizer, the PP/PET blend exhibits distinct two-phase morphology and the average particle size of the PET dispersed phase is about 1–2 μm. Owing to the immiscible nature of the blend, the poor interfacial adhesion is expectedly found as indicated by the pull out of the PET particles. As shown in [Figure 1(b)], with the addition of SEBS-*g*-MAH, the interfacial adhesion between the PP and the PET matrix is clearly improved and the average particle size is reduced to be 0.2–0.5 μm, suggesting the effectiveness of SEBS-*g*-MAH in compatibilizing PP/PET blend. Owing to the hydrophilic nature and interactions among the tubes, it has been demonstrated that HNTs were hard to well disperse in polymer by directly blending. As shown

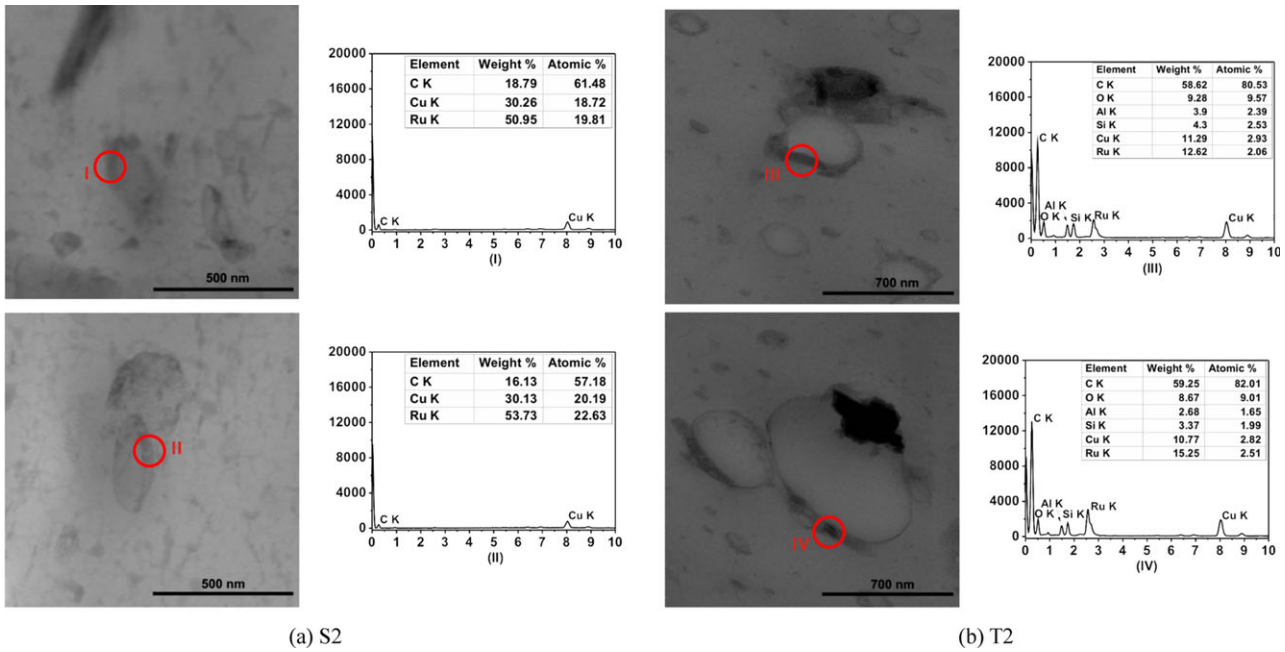

Figure 3. TEM micrographs and EDS analysis of the ultramicrotommed samples. [Color figure can be viewed in the online issue, which is available at wileyonlinelibrary.com.]

in [Figure 1(c)], when HNTs were attempted to add in PP/PET blend by single-step process, some aggregations of HNTs were inevitably formed. The aggregation may cause stress concentration and lead to poor mechanical properties. In two-step process, HNT aggregates, even dispersed HNTs, were hardly found in the fractured surfaces as shown in [Figure 1(d)]. It may be considered that HNTs are well dispersed in the polymer blend. To further illustrate the morphology of these blends, TEM observations were taken over the stained samples.

The TEM micrographs of *S2* and *T2* are compared in Figure 2. The observed oval dispersed phase is PET phase. The dark domain surrounding the PET phase is the SEBS-*g*-MAH owing to the staining effect. One can readily observe that the size of the PET domain is almost unchanged for the two methods. However, the location of HNTs is obviously different between the two samples. For the single-step method, oval-shaped PET phase is coated with SEBS-*g*-MAH layer. In addition, most of the HNTs are dispersed in PP phase randomly. Although for the two-step method, besides those of the PP phase, parts of HNTs are found to "coat" on the PET phase together with SEBS-*g*-MAH. Owing to the formation of such encapsulation structure, the oval-shaped PET phases became angular. To further substantiate the selective dispersion of HNTs in the interfacial region, TEM-associated EDS analysis was performed and the results are shown in Figure 3. The red-circled area of interfacial regions is subjected to EDS analysis. The results suggested that very limited silicon element could be detected in the interfacial regions of *S2*. Although in the interfacial regions of *T2*, additional aluminum (Al) and silicon (Si) were definitely detected. These characterizations provide further evidences on the selective dispersion of HNTs in the blend processed by two-step process.

The authors proposed an encapsulation model for the above-mentioned morphology, which is schematically shown in Figure 4. As the compatibilizer, SEBS-*g*-MAH possesses both polar groups and nonpolar olefin backbone. As a consequence, SEBS-*g*-MAH tends to locate in the interfacial region of PP/PET blend. As shown in [Figure 2(a)], SEBS-*g*-MAH would not coat the HNTs thermodynamically in the presence of PET. It seems

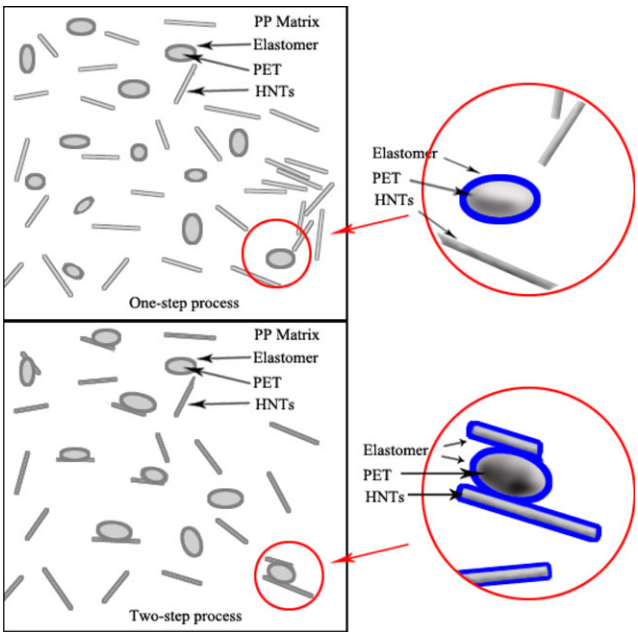

Figure 4. Schematic representation of encapsulation model (the blue layer is SEBS-*g*-MAH). [Color figure can be viewed in the online issue, which is available at wileyonlinelibrary.com.]

Applied Polymer SCIENCE

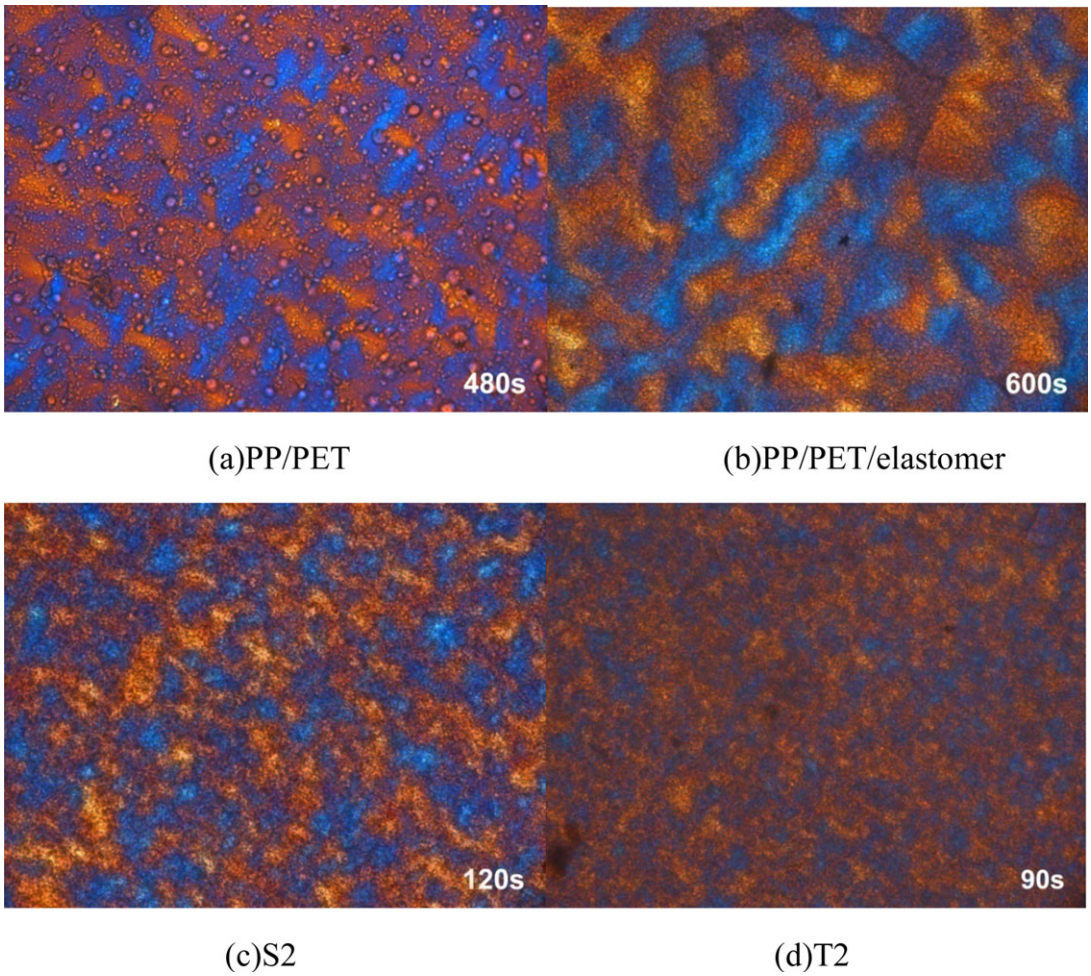

Figure 5. Comparison of spherulite evolutions of PP/PET blends at 120°C (magnitude, 500×). [Color figure can be viewed in the online issue, which is available at wileyonlinelibrary.com.]

to be that SEBS-*g*-MAH favors to coat the PET phase rather than HNTs. As a consequence, in the single-step method, most of the HNTs are dispersed in PP matrix without the compatibilizer in their interfacial region. The formation of HNT aggregates [Figure 1(c)] and poor interfacial bonding between HNTs and PP is expected to be detrimental for the mechanical properties, especially the toughness. In the two-step method, the HNTs are precoated with SEBS-*g*-MAH. Therefore, not only the interface between HNTs and PP is compatibilized, but also that between PET and PP is compatibilized by SEBS-*g*-MAH incorporated with HNTs. With such process, the interfacial bonding between PP and HNTs, and that between PET and PP is simultaneously improved. In addition, compared with the regular compatibilization with an elastomeric graft, in the two-step method, the interface between PP and PET is actually compatibilized with a hybridized substance consisting of the graft and nanosized inorganic tubes. In this situation, the transferring of stress from PP matrix to PET phase is supposed to be more effective owing to the reinforcing effective of HNTs toward SEBS-*g*-MAH. In addition, the SEBS-*g*-MAH located in PP/PET interphase becomes more rigid for the inclusion of HNTs, which is also supposed to be crucial for the retention of modulus of the compatibilized blends.

Crystallization Behavior of the Blend

To study the nucleation effects of HNTs on crystallization of PP/PET blends by using single-step process and two-step process, the evolutions of spherulites of PP/PET blends were observed via PLM under isothermal condition. Figure 5 shows the PLM photos of PP/PET blends crystallized at 120°C. From the images, it can be seen that with the incorporation of SEBS-*g*-MAH, the size of spherulites becomes much bigger and the crystallized time becomes much longer. With the addition of HNTs, much more spherulites grow and the sizes of spherulites become much smaller. Compared to two different methods of incorporation of HNTs, the two-step process possesses much quicker crystallization and much smaller size of spherulites. The facilitated crystallization and the finer crystallites could be explained by the heterogeneous nucleating effect of HNTs, which has been reported previously.[45] In the two-step method, the dispersing state of HNTs is more uniform, the crystallization time and crystallite size are consequently reduced.

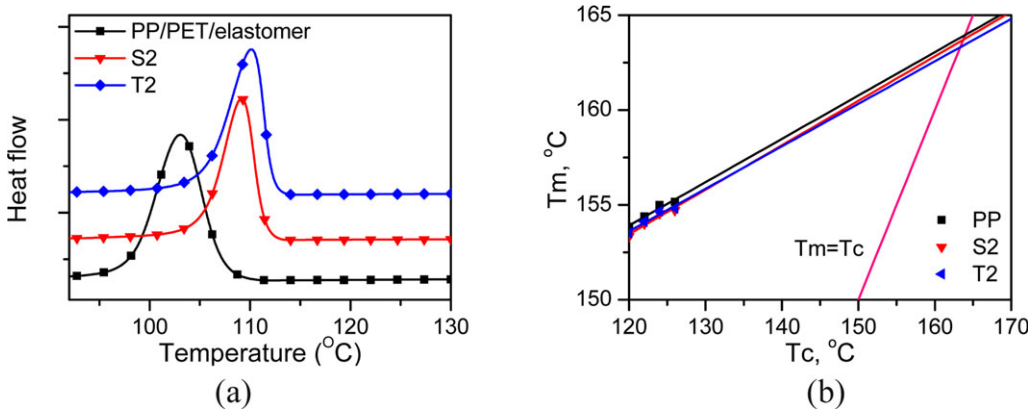

Figure 6. (a) Nonisothermal crystallization curves of PP/PET blends. (b) Melting temperature as a function of crystallization temperature for PP and PP/PET blends. [Color figure can be viewed in the online issue, which is available at wileyonlinelibrary.com.]

Figure 6(a) shows the nonisothermal crystallization process at 120°C for PP/PET blends. The peak temperatures and crystallinity of crystallization of PP and the PP/PET blends are summarized in Table I. Compared with PP/PET blend, the compatibilized one has much lower peak temperature for crystallization and the crystallinity is slightly increased. This is consistent with the observation from PLM result. After the inclusion of HNTs, owing to the nucleating effect, the crystallization peak temperature is shifted to higher value. Although the processing method can alter the crystallite morphology, it seems that it exerts limited effects on the crystallization temperature and crystallinity.

To uncover the potential effect of the processing method on the crystallization process, the isoconversional method was used to obtain the crystallization parameters with definite physical meaning. According to the Hoffman–Weeks theory, T_m^0 can be obtained by linear extrapolation of T_m versus T_c data to intersect the line $T_m = T_c$ and the intersection point is the T_m^0. In this study, the T_m^0 of PP and PP/PET blends is shown in [Figure 6(b)] and listed in Table II. Figure 7(a) shows the dependence of the effective activation energy on the relative extent of crystallization and the variation of the average temperature with the relative extent of crystallization obtained from the isoconversional method. As shown in [Figure 7(a)], it can be seen that at the same crystallinity, the absolute value of E_α of PP/PET blends with the incorporation of HNTs is always higher than that of neat PP. In addition, the absolute value of E_α of the PP/PET blends by two-step process is higher than that by single-step process. Furthermore, it can be seen that with the increase of crystallinity, all the absolute values of E_α of PP and PP/PET blends decrease.

In addition, the E_α–T curves were plotted to obtain the values of U^* and K_g by nonlinear fitting of eq. (5) and the results are shown in [Figure 7(b)] and Table II. The R^2 represents the dependency of the fitting curves and the data, the value of which is very close to 1, indicating the well fitting. As summarized in Table II, the values of σ_e for the composites are higher than that for neat PP, indicating higher folding surface energy of PP chains. The higher folding surface process indicated that PP chains are more difficult in crystallizing which may be caused by the hindrance effect of HNTs to the motion of PP chains. In the same volume of addition of 2 wt % HNTs, the value of σ_e by two-step process is found higher than that of single-step process. This is to imply that the hindrance effect of HNTs to the motion of PP chains is enhanced by two-step process.

Mechanical Performance

The mechanical properties of PP/PET blends are shown in Figure 8. As shown in Figure 8, we can see that, for both processing methods, the flexural and tensile strengths of the composites are increased consistently with HNT content. However, the addition of HNTs exerts detrimental effect on the toughness of PP/PET blends, in which the toughness is decreased with increasing HNT concentration. It has been reported that the incorporation of inorganics usually may dramatically reduce the impact strength of PP/PET composites.[46,47] Interestingly, the PP/PET blends prepared by two-step process exhibited

Table I. Nonisothermal Crystallization Parameters of Neat PP and PP/PET Blends

PP/PET/SEBS-g-MAH/HNTs	Crystallization enthalpy (J/g)	Crystallization temperature (°C)	Crystallinity (%)
PP	54.9	109.1	26.3
PP/PET	69.3	112.8	36.8
PP/PET/elastomer	68.4	103.1	38.2
S2	67.3	109.2	38.3
T2	70.0	110.1	39.8

Table II. Kinetic Data for Nonisothermally Crystallized of neat PP and PP/PET Blends

Sample	PP	S2	T2
U^* (J/mol)	4334.86	38,211.35	61,430.17
K_g (10^5K^2)	2.834	6.295	8.359
R^2	0.99463	0.99828	0.99716
T_m^0 (K)	437.15	436.85	436.45
$\sigma\sigma_e$ ($10^{-3}J^2/m^4$)	0.457	1.015	1.350
σ_e (J/m^2)	0.05197	0.1155	0.1535

Applied Polymer SCIENCE

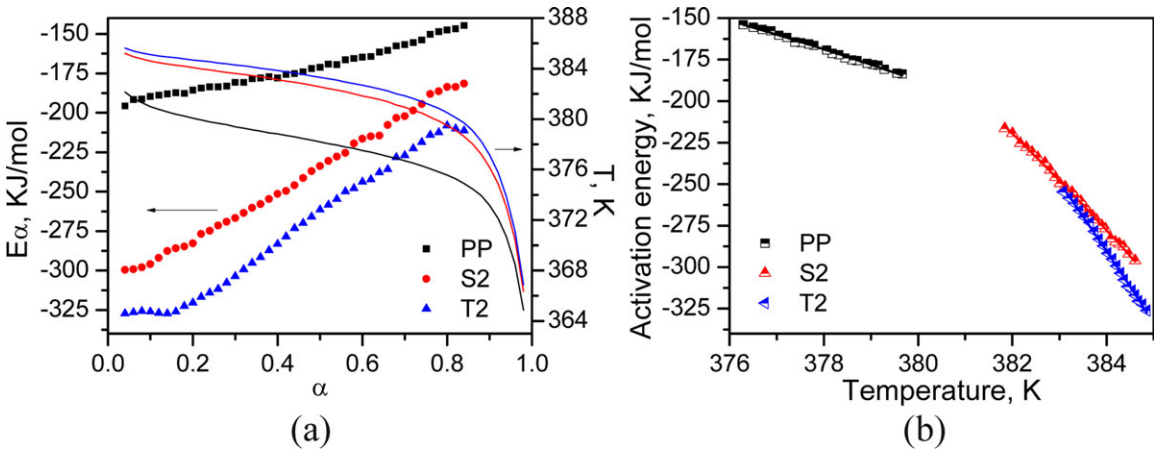

Figure 7. (a) Dependence of the effective activation energy on the relative extent of crystallization and the variation of the average temperature with the relative extent of crystallization (solid lines). (b) Dependence of the effective activation energy on average temperature and their fits of equation (solid lines). [Color figure can be viewed in the online issue, which is available at wileyonlinelibrary.com.]

remarkably higher flexural properties than those obtained by single-step process. For example, compared with *S0.5*, the flexural strength and flexural modulus of *T0.5* are increased by 14.0 and 12.2%, respectively. In addition, it is observed that the impact strength of the composites by the two-step process is also considerably higher than the single-step process especially when the concentration of HNTs is relatively higher. For example, compared with *S10*, the impact strength of *T10* is increased by 40%. It can therefore be concluded that mechanical properties of the samples prepared by two-step method are definitely superior to those of the samples by single-step processing.

Compared with single-step process, HNTs are first dispersed uniformly in the elastomer. The elastomer incorporated with

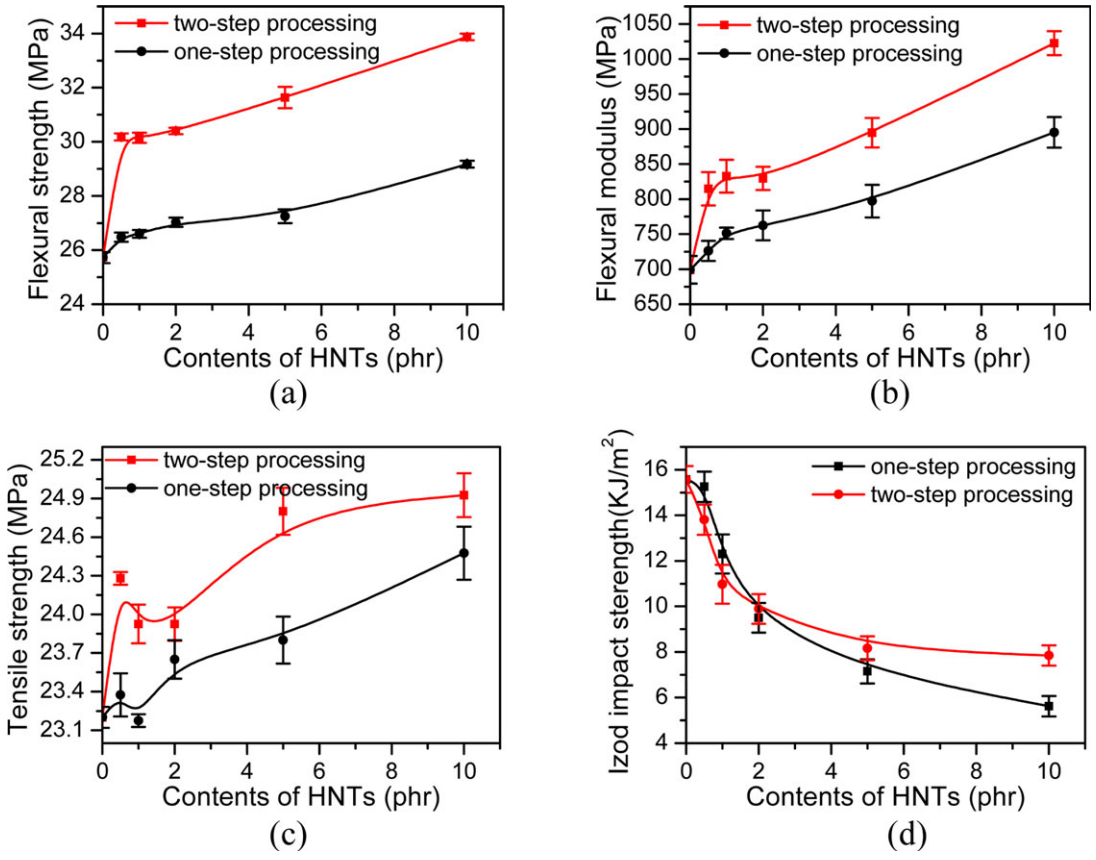

Figure 8. Comparison of the mechanical properties of PP/PET blends. [Color figure can be viewed in the online issue, which is available at wileyonlinelibrary.com.]

HNTs is partly dispersed uniformly in the PP matrix and partly selectively dispersed in the interface phase between PP and PET. With the coating of elastomer, HNTs could hardly reaggregate again, which is beneficial to enhancement of the toughness of the PP/PET blend. Furthermore, the selectively dispersed HNTs at the interphase improve the capability of stress transferring from PP matrix to PET phase as the interphase between PP and PET is mechanically stronger by incorporating HNTs. As the processing method does not change the crystallinity obviously, the formation of such unique morphology is crucial to the improvement of mechanical properties of the compatibilized PP/PET blends.

CONCLUSIONS

The selective dispersion of HNTs into the interfacial domain in a PP/PET blend (90/10) compatibilized by SEBS-*g*-MAH was realized by a two-step processing. Compared with the conventional single-step processing, the overall mechanical properties of the blend were substantially improved. The crystallization of PP in the blend was also facilitated by the selective dispersion of HNTs and the folding surface-free energy was substantially increased. The formation of the unique morphology was found to be crucial to the substantially improved mechanical performance. This study provides new insight in improving the performance of polymer blends via selectively dispersing the nanosized inorganics in the blend.

ACKNOWLEDGMENTS

This study was supported by National Natural Science Foundation of China (51222301 and 50933001), New Century Excellent Talents in University (NCET-10-0393), and Fundamental Research Funds for the Central Universities (2012ZG0002).

REFERENCES

1. Ke, F. Y.; Jiang, X. W.; Xu, H. Y.; Ji, J. L.; Su, Y. *Comp. Sci. Technol.* **2012**, *72*, 574.
2. Saujanya, C.; Radhakrishnan, S. *Polymer* **2001**, *42*, 4537.
3. Calcagno, C. I. W.; Mariani, C. M.; Teixeira, S. R.; Mauler, R. S. *Comp. Sci. Technol.* **2008**, *68*, 2193.
4. Tao, Y. J.; Pan, Y. X.; Zhang, Z. S.; Mai, K. C. *Eur. Polym. J.* **2008**, *44*, 1165.
5. Inoya, H.; Leong, Y. W.; Klinklai, W.; Thumsorn, S.; Makata, Y.; Hamada, H. *J. Appl. Polym. Sci.* **2012**, *124*, 3947.
6. Santos, P.; Pezzin, S. H. *J. Mater. Process Tech.* **2003**, *143*, 517.
7. Glor, M.; Muller, P.; Kubainsky, C. *Process Saf. Environ.* **2009**, *87*, 64.
8. Denk, R. *Trends Food Sci. Tech.* **2007**, *18*, S98.
9. Britton, L. G.; Holdstock, P.; Pappas, R. J. *Process Saf. Prog.* **2005**, *24*, 213.
10. Cheung, M. K.; Chan, D. *Polym. Int.* **1997**, *43*, 281.
11. Akbari, M.; Zadhoush, A.; Haghighat, M. *J. Appl. Polym. Sci.* **2007**, *104*, 3986.
12. Gartner, C.; Suarez, M.; Lopez, B. L. *Polym. Eng. Sci.* **2008**, *48*, 1910.
13. Pang, Y. X.; Jia, D. M.; Hu, H. J.; Hourston, D. J.; Song, M. *Polymer* **2000**, *41*, 357.
14. Oromehie, A. R.; Hashemi, S. A.; Meldrum, I. G.; Waters, D. N. *Polym. Int.* **1997**, *42*, 117.
15. Champagne, M. F.; Huneault, M. A.; Roux, C.; Peyrel, W. *Polym. Eng. Sci.* **1999**, *39*, 976.
16. Chiu, H. T.; Hsiao, Y. K. *J. Polym. Res.* **2006**, *13*, 153.
17. Papadopoulou, C. P.; Kalfoglou, N. K. *Polymer* **2000**, *41*, 2543.
18. Heino, M.; Kirjava, J.; Hietaoja, P.; Seppala, J. *J. Appl. Polym. Sci.* **1997**, *65*, 241.
19. Pracella, M.; Chionna, D.; Pawlak, A.; Galeski, A. *J. Appl. Polym. Sci.* **2005**, *98*, 2201.
20. Kawasumi, M.; Hasegawa, N.; Kato, M.; Usuki, A.; Okada, A. *Macromolecules* **1997**, *30*, 6333.
21. Chan, C. M.; Wu, J. S.; Li, J. X.; Cheung, Y. K. *Polymer* **2002**, *43*, 2981.
22. Rong, M. Z.; Zhang, M. Q.; Zheng, Y. X.; Zeng, H. M.; Walter, R.; Friedrich, K. *Polymer* **2001**, *42*, 167.
23. Ou, Y. C.; Guo, T. T.; Fang, X. P.; Yu, Z. Z. *J. Appl. Polym. Sci.* **1999**, *74*, 2397.
24. Premphet-Sirisinha, K.; Preechachon, I. *J. Appl. Polym. Sci.* **2003**, *89*, 3557.
25. Ma, C. G.; Mai, Y. L.; Rong, M. Z.; Ruan, W. H.; Zhang, M. Q. *Comp. Sci. Technol.* **2007**, *67*, 2007.
26. Premphet, K.; Horanont, P. *J. Appl. Polym. Sci.* **2000**, *76*, 1929.
27. Brindley G. W. Crystal Structures of Clay Minerals and Their X-ray Identification; Mineralogical Society: London, **1980**, p 1.
28. Du, M. L.; Guo, B. C.; Jia, D. M. *Eur. Polym. J.* **2006**, *42*, 1362.
29. Ye, Y. P.; Chen, H. B.; Wu, J. S.; Ye, L. *Polymer* **2007**, *48*, 6426.
30. Liu, M. X.; Guo, B. C.; Du, M. L.; Lei, Y. D.; Jia, D. M. *J. Polym. Res.* **2008**, *15*, 205.
31. Liu, M. X.; Guo, B. C.; Zou, Q. L.; Du, M. L.; Jia, D. *Nanotechnology* **2008**, *19*, 205709.
32. Ismail, H.; Pasbakhsh, P.; Fauzi, M. N. A.; Abu Bakar, A. *Polym. Test.* **2008**, *27*, 841.
33. Hedicke-Hochstotter, K.; Lim, G. T.; Altstadt, V. *Comp. Sci. Technol.* **2009**, *69*, 330.
34. Guo, B. C.; Chen, F.; Lei, Y. D.; Liu, X. L.; Wan, J. J.; Jia, D. M. *Appl. Surf. Sci.* **2009**, *255*, 7329.
35. Du, M.; Guo, B.; Lei, Y.; Liu, M.; Jia, D. *Polymer* **2008**, *49*, 4871.
36. Brandrup, J.; Immergut, E. H.; Grulke, E. A. Polymer Handbook; Wiley: New York, **1989**.
37. Hoffman, J. D.; Davis, G. T., Lauritzen, J. I. Treatise on Solid State Chemistry; Hannay, N. B., Ed.; Plenum Press: New York, **1976**; Vol. *3*, p 497.

38. Xiao, W.; Wu, P.; Feng, J. *J. Appl. Polym. Sci.* **2008**, *108*, 3370.
39. Vyazovkin, S.; Sbirrazzuoli, N. *Macromol. Rapid Commun.* **2004**, *25*, 733.
40. Marand, H.; Xu, J.; Srinivas, S. *Macromolecules* **1998**, *31*, 8219.
41. Vyazovkin, S.; Dollimore, D. *J. Chem. Inf. Comp. Sci.* **1996**, *36*, 42.
42. Vyazovkin, S. *J. Comput. Chem.* **1997**, *18*, 393.
43. Vyazovkin, S. *J. Comput. Chem.* **2001**, *22*, 178.
44. Doyle, C. D. *J. Appl. Polym. Sci.* **1962**, *6*, 639.
45. Du, M. L.; Guo, B. C.; Wan, J. J.; Zou, Q. L.; Jia, D. M. *J. Polym. Res.* **2010**, *17*, 109.
46. Chow, W. S.; Ishak, Z. A. M.; Karger-Kocsis, J.; Apostolov, A. A.; Ishiaku, U. S. *Polymer* **2003**, *44*, 7427.
47. Wang, H.; Zeng, C. C.; Elkovitch, M.; Lee, L. J.; Koelling, K. W. *Polym. Eng. Sci.* **2001**, *41*, 2036.